MAY/JUNE | EMEA | ISSUE 54

WILEY

# MICROSCOPY AND ANALYSIS

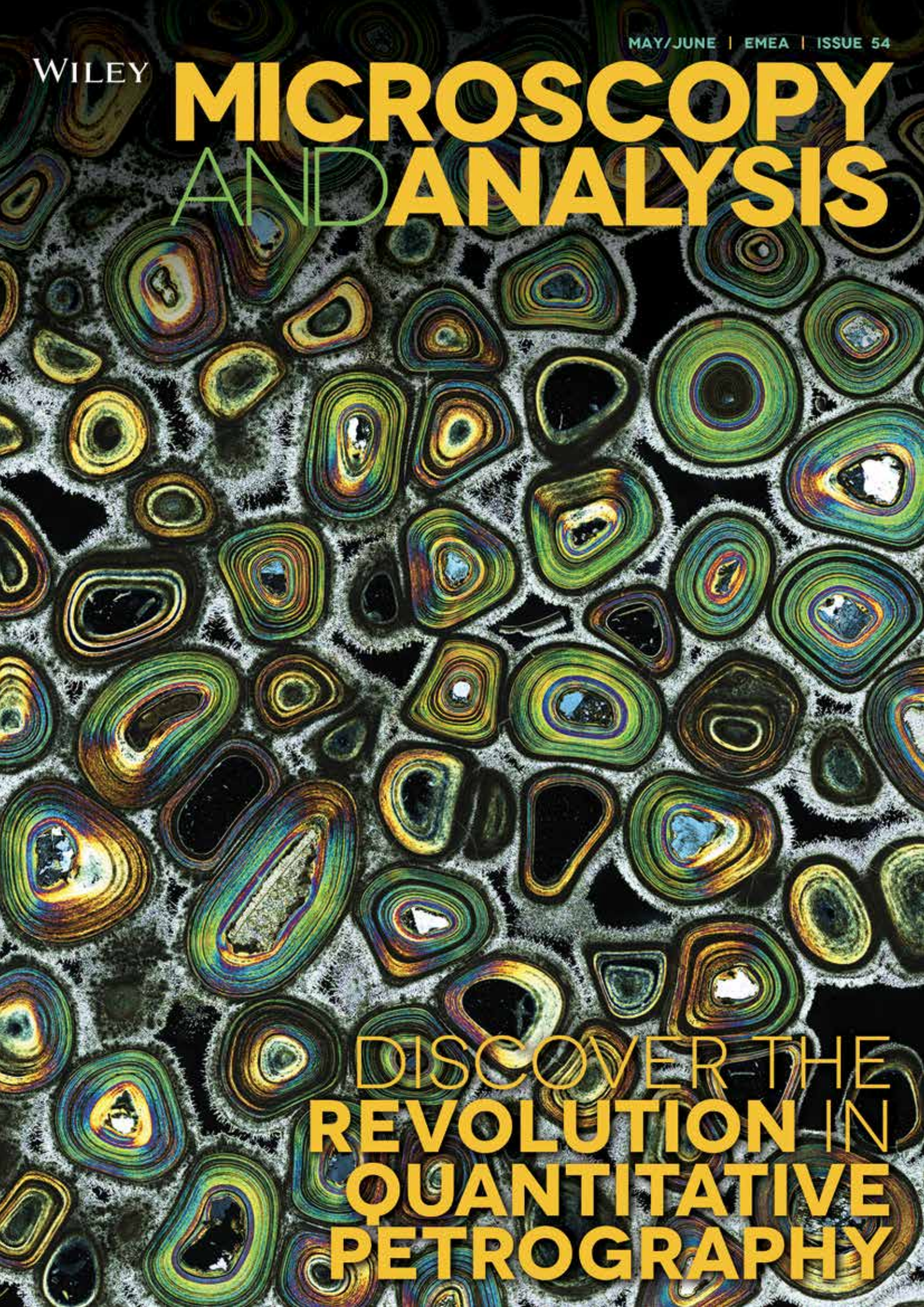

## DISCOVER THE REVOLUTION IN QUANTITATIVE PETROGRAPHY

# Direct electron and X-ray detection with pixelated detectors

**LOTHAR STRÜDER[1,3]*, STEFAN ASCHAUER[1], PETER HOLL[1], ROBERT HARTMANN[1], MARTIN HUTH[2], PETRA MAJEWSKI[2] AND HEIKE SOLTAU[2]**

1 PNSensor GmbH, Otto-Hahn-Ring 6, 81739 München, Germany
2 PNDetector GmbH, Otto-Hahn-Ring 6, 81739 München, Germany
3 University of Siegen, Walter-Flex Str.1, 51228 Siegen, Germany

**BIOGRAPHY**

Lothar Strüder is CEO and co-founder of PNSensor, performing research and development of advanced radiation detectors. He holds a PhD in physics from the Technical University of Munich and a professorship in physics at the University of Siegen. His research interests comprise the study of the limits of measurement precision of ionizing radiation with semiconductor detectors. He's published more than 450 papers and given over 500 contributed and invited talks. Prominent projects he's led include the development of position, energy and time resolving detectors for astronomy and astrophysics, synchrotron and X-ray free electron laser experiments and state-of-the-art lab instrumentation. He's also received many awards for his work.

**ABSTRACT**

The direct detection of ionizing radiation is the most precise technique to get simultaneously the highest signal-to-noise ratio for the measurement of position, energy and time. This holds for bolometric, magnetic and charge generating detectors. We restrict our discussion to sensor technologies capable to be operated close to room temperature. Small band gap materials deliver the best spectroscopic performance but need to be cooled to low temperatures. Wide band gap materials can operate at room temperature but generate less signal charges per absorbed energy. Silicon is a good compromise between the two extremes: it requires only moderate cooling and still delivers a large number of signal charges due to its band gap in the eV range. In addition, the signal charge carrier lifetime is very high. This article describes the emergence of position, energy and time resolving silicon sensors for the direct detection of electrons and X-rays in the field of microscopy and microanalysis as a tool for the study of the structure and dynamics of matter. It is focused on the fast and precise detection of electrons up to 300 keV and of X-rays from 50 eV to 30 keV. Special attention is given to performance figures like energy resolution, spatial precision, dynamic range and quantum efficiency.

**CORRESPONDING AUTHOR**
lothar.strueder@pnsensor.de

## INTRODUCTION

In most classical microscopy applications, light from the near infrared (E ≈1 eV) through the visible domain (E ≈ 2 eV) and up to the near UV spectrum (E ≈ 3 eV) is used. In this energy range dedicated, mostly silicon-based sensors with pixel sizes on the scale of a few microns and formats up to 8k x 8k pixels are commercially available at moderate cost [1]. Within the above-mentioned range of photon energies every incoming photon generates one electron-hole pair through the photoelectric effect in silicon[2]. The photons of the visible spectrum (1.5 eV to 2.5 eV) are stopped in the silicon within the first 5 µm. High quantum efficiency can be easily achieved with current state-of-the-art CMOS technologies with a depletion i.e., sensitive depth of a few microns.

The direct detection of X-rays in the energy range from 50 eV up to 30 keV or electrons with energies up to 300 keV however needs a much larger sensitive volume to efficiently absorb the incident radiation.

The proper detection of ionizing radiation succeeds best if the incident particles or photons deposit their entire energy in the active volume of the sensor. The detection of photons in silicon in the energy range from 1 eV to 30 keV is dominated by the photoelectric effect resulting in an energy dependent number of signal charge carriers, i.e., electron-hole pairs. The absorption cross section is a complex function of the atomic structure of the sensor material resulting in an absorption depth of a few nm only for X-rays around 100 eV up to an absorption depth of 1 mm at an X-ray energy of 20 keV in silicon as the detector material.

Non-relativistic energetic electrons however undergo multiple inelastic scattering as soon as they enter the silicon sensor. Close to the end of their track in the sensor material the remaining electron energy is deposited in a small volume due to the increasing interaction cross section[3].

The scope of our article is based on detector schemes having the potential to fully absorb the energy of the incoming radiation, to cope with absorption depths over more than four orders of magnitude and to perform simultaneous energy, intensity and position measurement at high speed with a large dynamic range. Therefore, we restrict the scope of detectors to fully depleted imagers with extremely thin intrinsic radiation entrance windows. The detectors should be able to operate close to room temperature because most applications in the field require easy-to-use equipment – robust and compact.

The detection of ionizing radiation was revolutionized in the early eighties through the development of a planar process for very high resistivity silicon needed for the fabrication of sensors and by the invention of the principle of sideward depletion[4, 5]. After explaining the basic concepts of the sensor systems, we will describe the capabilities of the detectors and their physical limitations with respect to the measurement precision. Most importantly, we will introduce several representative applications of such detectors in Heaven (space) and on Earth (ground).

## THE PHYSICAL CONCEPT OF FULLY DEPLETED SENSORS

Since the invention of the principle of sideward depletion in 1983[4], silicon drift detectors (SDDs), pnCCDs and DePFET active pixel sensors have had a great impact in the field of radiation detection. One decade before, Boyle and Smith invented the charge coupled device (CCD)[6] for imaging and signal processing purposes. The transfer of signal charges in a CCD was performed by rapidly changing voltages of isolated shift electrodes on the surface of the CCD to create time variant potential wells inside the semiconductor to transfer the signal

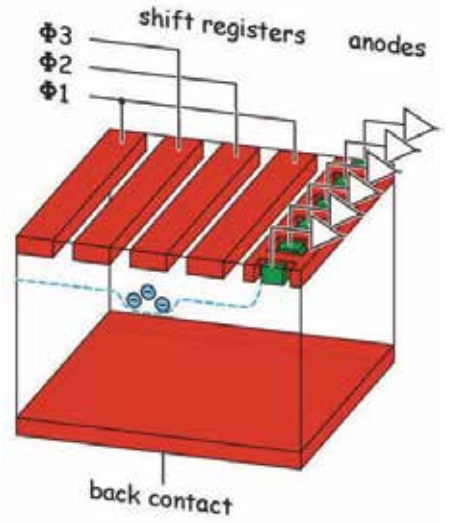


**FIGURE 1** *Schematic representation of a pnCCD. Both surfaces are covered with rectifying $p^+$ implants (red) of a high resistivity n-type silicon wafer. The upper side is subdivided into $p^+$ strips with every third strip connected to the same voltage. The voltages are chosen such that a potential minimum for electrons forms under the most positively biased $p^+$ strip. A periodic change of the applied voltages guarantees the persistence of a locally varying potential minimum guiding the signal electrons to the $n^+$ readout node (green).*

Microscopy and Analysis 35(3): 16-21 (EU), May 2021

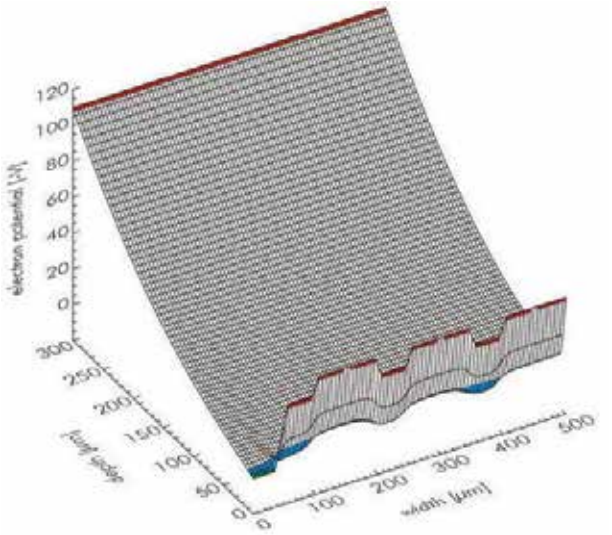


**FIGURE 2** *2D electron potential of a pnCCD obtained through device simulations. All p⁺ contacts (red) are negatively biased with respect to the readout node at position 0,0. The strongly negatively biased p⁺ back contact shifts the potential minimum towards the side having the pixel structure where the changing voltages on the p+ strips create the local potential minima for electrons and shift them pixel by pixel towards the readout node.*

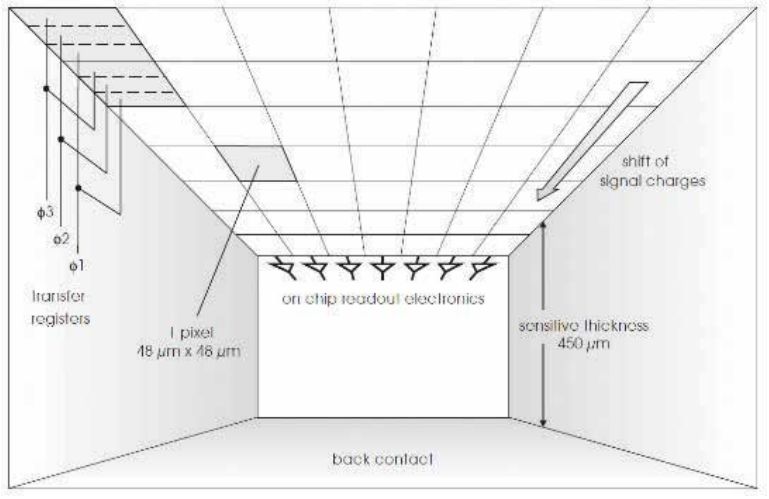


**FIGURE 3** *The pnCCD seen from the inside. The ionizing radiation enters the detector from the back side and converts in the silicon bulk to electron-hole pairs. The holes are absorbed by the back contact the electrons move close to the surface with the pixel structure where they are shifted towards the end of the pnCCD column. An integrated JFET amplifier at the end of each column changes the impedance of the signal from GΩ to kΩ. The column-parallel signals of the JFETs on the pnCCD is received by an ASIC for further signal processing.*

charges from their point of creation to a read-out node. In contrast to this approach, Rehak and Gatti were exploring a constant drift field such that the detector could be operated in a DC mode without changing voltages. To highlight the similarities and differences of the two devices Rehak called the SDD a phase-less CCD and in contrast the pnCCD a discretely transferring SDD.

## SIDEWARD DEPLETION

A double sided polished high resistivity n-type silicon wafer can be entirely depleted from mobile charge carriers if both wafer surfaces are covered with rectifying p+ junctions (see Figure 1). Only a very small n+ implanted contact is needed as an ohmic access to the silicon sensor to apply a reverse bias voltage and drain off all mobile charge carriers. In this configuration the depletion occurs from both wafer surfaces from the p+- regions until the detector volume is completely sensitive. The n+ node is then the most positive point in the detector structure where all the signal electrons will be collected (at the x-y position 0,0 in Figure 2). This way the depleted sensitive detector area becomes independent of the detector´s read node capacitance. The signal electrons generate a voltage swing ΔV at the collecting node which is proportional to the number of electrons according to ΔV = ΔQ/C (ΔV is the voltage swing, ΔQ the amount of signal charge and C the total node capacitance). For example, a 40 fF node capacitance directly coupled to a transistor yields a voltage change of 4 µV for every collected electron.

## ELECTRONIC NOISE AND ENERGY RESOLUTION

As can be seen from equation (1) the noise or better the equivalent noise charge ENC expresses the influence of various physical noise sources on the total noise of a detector readout as a function of detector and transistor parameters. It can be understood as the number of fluctuating electrons you have to inject into the input of your amplifier to generate the measured total noise at the output.

$$ENC=\sqrt{\alpha\frac{2kT}{g_m}C_{tot}^2A_1\frac{1}{\tau}+2\pi a_f C_{tot}^2A_2+qI_LA_3\tau} \quad (1)$$

In equation (1) k is the Boltzmann constant, T the temperature, α is a parameter describing the input noise source, $g_m$ the transconductance of the first transistor, A1, A2 and A3 are constants describing the frequency depending filtering, $a_f$ parametrizes the so-called "low frequency noise", q is the elementary charge, and $I_L$ is a DC electron current, e.g. the thermally generated leakage current or dark current. The first term under the square root is called the series noise and scales with $C_{tot}^2$ and $\frac{1}{\tau}$. That means if the total input capacitance is large, the series noise increases. For a given capacitance C the noise contribution can be reduced only by either extending the signal processing time τ, with the consequence of reading out the signals at a low rate, or by increasing $g_m$ of the first transistor. The second term is independent from the signal processing time τ, but again proportional to the total input capacitance $C_{tot}^2$. Both components, the series noise and the low frequency noise, heavily profit from a low input capacitance. The last term is independent of the total input capacitance but proportional to the signal processing time τ. It is depending on the thermally generated leakage current or dark current and can be reduced by an appropriate operating temperature and an optimized sensor fabrication technology. As a summary: if you want to readout fast at a low noise level, the total input capacitance must be minimized. To obtain the system energy resolution, the noise contribution from equation (1) has to be quadratically added to the Fano noise (eq. 2) caused by statistical fluctuations in the ionizing process:

$$ENC_{fano}=q\cdot\sqrt{\frac{F\cdot E_x}{w}} \quad (2)$$

where F is the Fano factor in silicon (F = 0.115), $E_x$ is the X-ray energy and *w* is the average pair creation energy (in silicon *w* = 3.68 eV at room temperature). The Fano contribution to the FWHM describes the theoretically achievable lower limit of the energy resolution.

## POSITION RESOLUTION

The position precision in fully depleted pixelated detectors is dominated by several parameters: (a) electronic readout noise, (b) drift time of the signal charges from their point of conversion until confined in the potential wells of the pixel structure, (c) operating temperature, (d) X-ray energy, and, of course, (e) the physical pixel size. Once an X-ray is absorbed in the silicon through the photo-effect (most probable conversion process up to 50 keV), a signal charge cloud is generated in a small volume. Electrons and holes are separated by the electric field in the detector. The electrons move to the most positive point in the sensor volume (i.e., the pixel structure in a CCD or any attractive n-type location) while the holes move to the most negative contact, e.g., the negatively biased p⁺ back contact.

The small electron charge cloud, just after being generated by the incoming X-ray, is subject to three different processes: (a) drift to the potential minimum through the electric field applied for the depletion of the sensor, (b) electrostatic repulsion and (c) diffusion mainly in the direction perpendicular to the drift motion. In a typical detector configuration, a point-like initial charge cloud generated by a 1.5 keV X-ray will expand to a gaussian radial electron distribution σ of more than 10 µm (rms). That means, in case of a low noise pixelized detector with a pixel size of 48 µm × 48 µm most of the electron charge clouds will be spread over more than one pixel. A centroiding of the charge content of the hit pixels improve the position precision dramatically as the following example shows: At an X-ray energy of 1.3 keV impinging on a pnCCD with a pixel size of 48 µm, the position precision improves to better than 3 µm (rms)[7]. The overall position response function of the sensor to X-rays is complex and requires careful simulation and calibration of the detector system.

## FULLY DEPLETED BACK ILLUMINATED PNCCDS

The principle of sideward depletion was first successfully applied to silicon drift detectors[8]. However already the very first paper discussing sideward depletion[4] mentioned the possibility to use it equally for fully depleted pnCCD type detectors. The working principle is of a pnCCD is shown in Fig. 1. The volume of the high resistivity n-type silicon bulk is depleted through the p⁺ implants on either side: p⁺ shift registers (red) and p⁺ back contact (red) symmetrically biased against the tiny n⁺ readout nodes (green). An additional negative voltage is applied on the back contact to shift the potential minimum for electrons close to the side having the shift registers forming the pixel structure. The applied voltages on the three shift registers are chosen such that a local potential minimum for electrons is formed. A change in time of the voltages on the registers allows electrons collected in the time variant potential minimum to move towards the readout node. A typical potential distribution is shown in Fig. 2 where the electrons are collected in the local potential minima (blue) on the side having the pixel structure

and the holes would be absorbed in the rectifying $p^+$ back contact (red). A view from the pnCCD inside is depicted in Fig.3. The 450 µm fully sensitive silicon bulk is the absorbing volume for the radiation impinging on the detector from the back contact side. The electrons move to the top side of the pnCCD finally confined in the pixel structure. The signal charge packages are transferred discretely column-parallel wise to the end of the pixel structure. An integrated low noise n-channel JFET amplifier at the end of each CCD column receives the signal charges and converts the high impedance signal in a low impedance, robust output. A conventional CCD requires for the readout and signal processing typically $n^2$ readout cycles (e.g., a matrix of n × n pixels) while the fully column parallel pnCCD reduces the simultaneous number of signal processing to n cycles only. Therefore, the readout time of a low noise pnCCD frame is n times faster compared to the readout of conventional CCDs.

A large variety of pnCCDs with different formats and pixel sizes have been developed for scientific and industrial applications: X-ray astronomy, adaptive optics, synchrotron and X-ray FEL experiments, material science, transmission electron microscopy, channeling physics, high energy physics, plasma physics and numerous laboratory set-ups. pnCCDs with sensitive thicknesses of 280 µm to 450 µm have been fabricated, with pixel sizes from 36 µm × 36 µm to 150 µm × 150 µm and formats up to 1056 x 1056. The full frame rates ranged from 120 frames per second (fps) at the X-ray FEL at LCLS with 1056 x 1056 pixels[14] up to 2.000 fps in the TEMs with 264 x 528 pixels. As on-chip binning and windowing can be applied more than 10,000 fps have been demonstrated with such devices.

The properties of one representative example of a commercially available pnCCD system as installed in numerous TEMs, beamline endstations and laboratory set-ups are shown in Table 1, above right.

The above properties allow for X-ray imaging with Fano limited energy resolution and high speed, high dynamic range imaging of electrons in SEMs and TEMs. In the following we will describe a variety of scientific and industrial applications where the high speed, high spatial resolution and the very low noise operation for Fano limited energy resolution was essential.

## X-RAY ASTRONOMY

Right after the invention of the SDD in 1983 the European Space Agency received a proposal from the astrophysics community in 1984 to develop and launch a satellite with large Wolter-type X-ray telescopes with long focal length to image X-rays from 100 eV to 10 keV from celestial objects. The astrophysical specifications for such a mission were ideally fitting to the potential properties of the SDD based concepts: spatial resolution matched to the X-ray optics, Fano-limited energy resolution, high speed operation for the observation of transient sources, long-term stability and radiation hardness and last not least high quantum efficiency for highest sensitivity. In 1999 XMM-Newton was launched from Kourou, ESAs space port in French Guiana. The pnCCD focal plane is still operating within specification after 22 years in orbit. It survived a micrometeorite impact and its sensitivity is unchanged since launch.

The X-ray telescope on XMM with the highest X-ray throughput was equipped with a monolithic pnCCD as shown in Fig. 4. A 6 cm × 6 cm monolithic pnCCD was fabricated defect-free on a 100 mm double sided polished high resistivity float zone silicon wafer. 400 × 400 pixels, 150 µm × 150 µm in size are read out 100 times per second with spectroscopic quality, as shown in Fig. 5. Every single X-ray emitted from the supernova remnant Tycho Brahe in Fig.5 and imaged through the telescope has been resolved in time, position and energy. The continuum spectrum in Fig. 5 allows to measure the temperature of the remnant while the abundances of fluorescence X-rays of O, Ne, Si, Mg, Ar, S, Ca and Fe and their spatial distribution within the remnant reveal details of this astrophysical event. The mechanisms and dynamics of this supernova explosion were analyzed in detail in[9]. Up to now approximately one million new X-ray sources have been discovered, more than 7,500 scientific publications based on XMM data were published, the pnCCD paper[10] was cited more than 2,000 times. The pnCCD development for the XMM-Newton mission is considered as one of the most successful instrument innovations in X-ray astronomy. pnCCDs have been integrated in three more X-ray astrophysics missions.

| | |
|---|---|
| **Physical pixel size** | 48 µm × 48 µm × 450 µm |
| **Number of physical pixels** | 2 × 264 × 264 (139,392) imaging + frame store area |
| **Active area** | 2 × 12.7 mm × 12.7 mm (322 $mm^2$) imaging + frame store area |
| **Imaging frame rate** | up to 1,000 Hz (264 × 264 pixel) |
| **Pixel readout rate** | up to 70 Megapixels/s |
| **Windowing mode** | 24 × 264 pixels (smallest window) |
| **Externally triggerable** | yes |
| **Readout noise (rms)** | ENC typ. $3e^-$ – $4e^-$ / pixel at 400Hz |
| **Energy resolution** | 140 eV for Mn-$K_\alpha$ at 5.9 keV |
| **Sub-pixel spatial resolution** | $\Delta x < 3$ µm (rms) for 1.3 keV X-rays [7], i.e., 18 × $10^6$ pixels |
| **Charge handling capacity** | up to 600,000 signal electrons per pixel |
| **Radiation hardness** | up to $10^{14}$ photons/$cm^2$ at 10 keV |

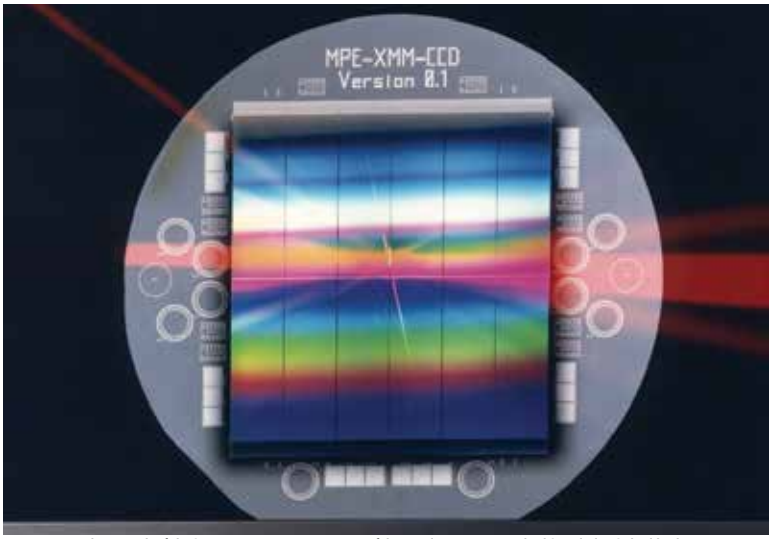


**FIGURE 4** *Photograph of the largest X-ray CCD (up to 1999) fabricated on a 100 mm double-sided polished high resistivity float zone silicon wafer. The pnCCD itself has an area of 6 cm x 6 cm with 400 x 400 pixels of a size of 150 µm x 150 µm ideally matched to the X-ray telescope angular resolution.*

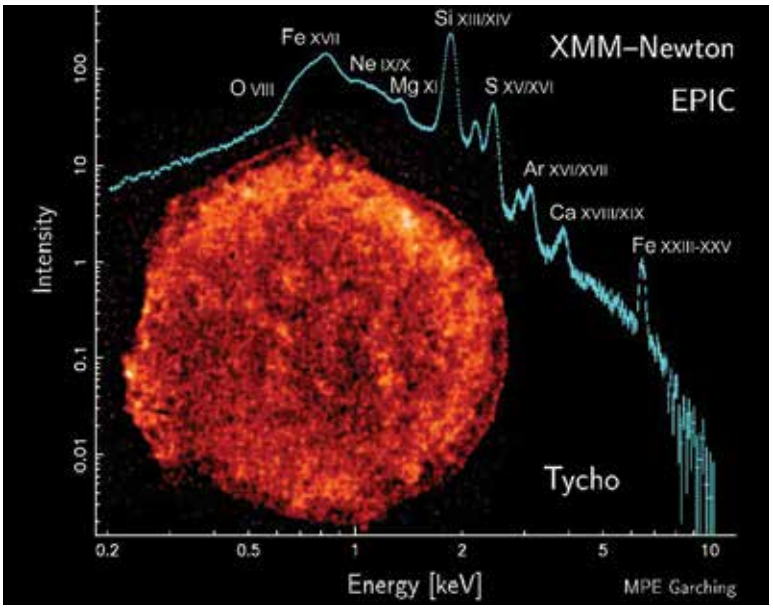


**FIGURE 5** *X-ray image of the supernova remnant Tycho Brahe. Every single photon is recorded in terms of energy, position and arrival time. The spatially resolved spectral composition allows to model and analyze the element evolution and dynamics of the supernova explosion.*

## SYNCHROTRON AND XFEL EXPERIMENTS

X-ray imaging experiments at synchrotron and X-ray Free Electron Laser facilities (XFELs) are mainly performed in two different ways:

### *1* COUNTING MODE

Monochromatic radiation is diffracted or scattered from a sample and recorded on a 2D imaging detector. As the energy $E_x$ of the X-ray is precisely known, the integrated signal charge of many absorbed X-ray photons in a pixel of the detector divided by the number of electron-hole pairs generated by one incident X-ray photon ($Ex/w$, $w$=3.68 eV at room temperature) gives the number of hits in a pixel, i.e. the X-ray intensity. When the arrival of the incident photons is separated in time more than approx. 100 ns, an in-pixel counter can be operated to record all events above a well-defined threshold, increasing the counter by one each time a signal above threshold is detected.

### *2 SPECTROSCOPIC MODE:*

A second type of experiments uses a white or pink (non-monochromatic) X-ray beam and makes directly use of the intrinsic energy resolution of the detectors. In this case the detector is operated in a single X-ray recording mode: Every isolated pixel pattern ("event") generated by the signal charge cloud of an absorbed X-ray photon is spatially or temporally separated from other events. By summing up the amplitudes in the vicinity of the seed pixel the total energy deposition of the event can be measured with a precision given by the limits of the Fano-processes and the electronic noise (see eqn. (1) and (2)). Event pile-up and pattern pile-up have to be avoided to maintain the excellent energy resolution. Both types of operation modes are frequently used at synchrotrons and XFEL experiments.

## SYNCHROTRON EXPERIMENTS

In most of the synchrotron experiments

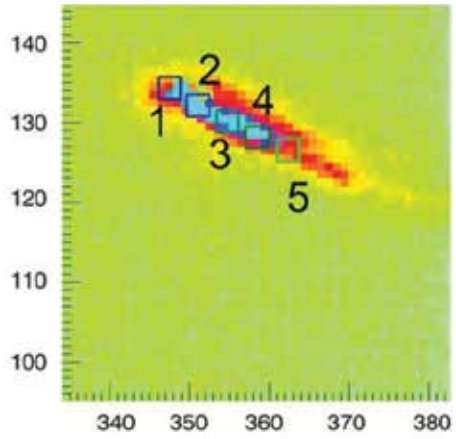


**FIGURE 6** *A focused pink X-ray beam (500 x 500 nm²) is hitting a Cu sample at spot (511) in a region of high mechanical stress. In areas with no stress the Laue-spot has a round shape covering a few pixels only. The high stress region however shows a widening of the peak and an extended elongation. In addition, the energy between the measured areas 1 to 5 show a shift in energy indicating strong perturbation of the Cu lattice[11].*

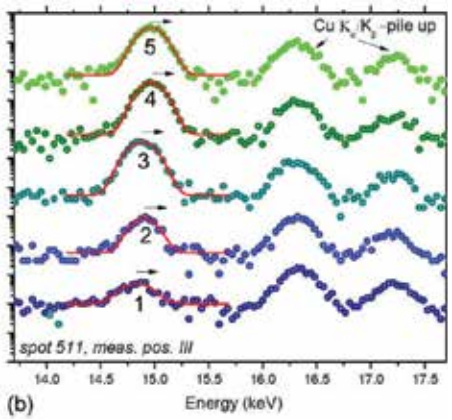


**FIGURE 7** *The analysis of the heavily distorted Laue-spot in the 511 direction shows a heavy streaking and a shift in energy along the streak from the indicated positions 1 – 5 in Fig 6 of the order of 50 eV. This indicated a change of lattice spacing change due to the induced stress at that position.*

the X-rays hitting the sample under test are scattering X-rays into a pixel of a 2D focal plane detector on a sub-microsecond time scale. By reading $10^5$ pixel of a detector (see Table 1) 1000 images per second results in an achievable total count rate of $10^6$ X-rays per second if the occupancy of the detector is limited to 1% in order to avoid pile-up for spectroscopic measurements. In case only the integral number of monochromatic X-rays per pixel is needed the X-ray flux can be a factor of $10^5$ higher. In that case the energy information of the X-ray is lost but the imaging capabilities are maintained.

## EXAMPLE OF SYNCHROTRON MEASUREMENTS IN THE SPECTROSCOPIC MODE: FATIGUE ANALYSIS OF METALS

The energy dispersive Laue diffraction (EDLD) method allows to record Laue spots of a sample and to profile their spatial and energetic structures at the same time[11].

This technique is by far faster and more accurate than what is otherwise available. It is a convincing example for the use of spectroscopic imaging detectors for synchrotron experiments. Continuous scans of a sample surface can be performed without interruptions to measure position and energy coordinates of a diffracted Laue pattern simultaneously as a function of the probed sample volume. Moreover, the unperturbed incident beam allows for a well-defined and sharply localized foot print of the beam on the sample.

Compared to many other techniques, neither the precise knowledge of the incident energy spectrum nor modifications of the spectrum upstream or downstream of the experimental setup such as monochromators or energy filters are required for a successful Laue diffraction experiment if an energy-dispersive CCD is used. Analytical calculations can predict the Laue spots' energies with the knowledge of the primary beam spectrum and the angle of incidence in the case of perfect crystals only.

For deformed crystals, the diffracted energies will shift in unpredictable manners. However, a measurement of such shifts is only possible if either the incident energy is precisely known and scanned over the required energy range or if an energy-dispersive area detector is used for Laue diffraction (see Fig. 6)

The EDLD method establishes a new step in structural analyses of materials since deviatoric strains and interplanar spacing distances {dhkl} can be determined simultaneously. This allows broadening the application scope of stress measurements to multi grain samples with higher orientation gradients. In the future EDLD performed with novel energy dispersive imaging detectors like the pnCCD will be used to determine macroscopic strains (of the first order) in elastically stressed samples, provided that a sufficient number of Bragg peaks is measured.

An analysis of the streaking behaviour (see Figs. 6 and 7) can serve as an important tool to distinguish between structural effects accompanying plastic deformation of crystals and to understand the deformation behaviour of crystals at the micrometer and the sub-micrometer scale. Methodologically, the new approach allows for an straightforward study of strain distributions in small crystalline domains using white-beam X-ray diffraction.

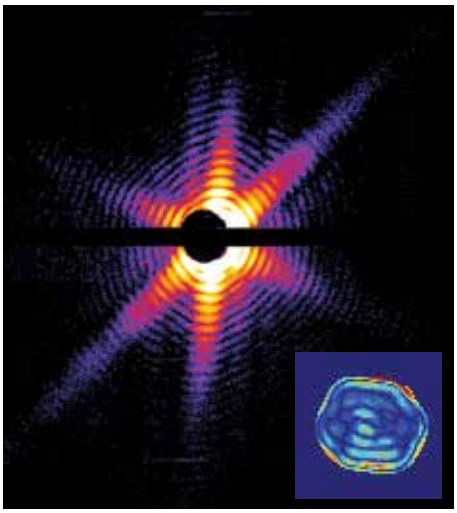

**FIGURE 9** *Diffraction image of a biological sample (Mimivirus)[13]. A large dynamic range is required for a proper detection of the pattern: From no or one X-ray in a pixel up to 500 in one pixel in the center. The small insert at the lower right is the reconstructed Mimivirus with a spatial resolution of the order of 20 nm.*

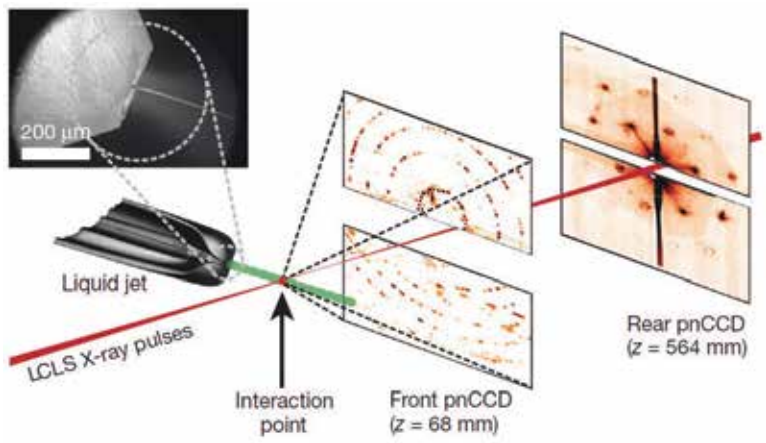


**FIGURE 8** *The experimental concept of the end station AMO at LCLS on the SLAC campus in Menlo Park. Nanocrystals or biological samples are injected in a vacuum chamber through a liquid jet. The focused LCLS X-ray pulse interacts with the nanocrystals in the liquid or gas jet and eventually hits the samples in the sample beam. In the case of nanocrystals of the Photosystem I a powder diffraction type pattern is recorded on the front pnCCD 68 mm behind the interaction point. The small angle scattering on the rear pnCCD 564 mm away from the interaction point indicates the size of the nanocrystals from 100 nm up to 800 nm[12].*

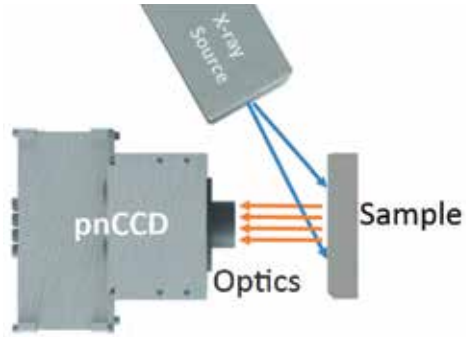


**FIGURE 10** *Experimental set-up for a full field XRF measurement using polycapillary optics and a pnCCD. For energies above 2 keV the measurements can be performed at ambient conditions without vacuum. The polychromatic light from the X-ray source excites the atoms of the sample and finally leads to the emission of fluorescence X-rays. The polycapillary optics with bundles of typically 5 µm – 10 µm Ø act as a wave guide and conserves the location of the emitting atom in the image of the X-ray camera. An elemental map of the sample surface can be generated without moving parts or scanning beams.*

## X-RAY FREE ELECTRON LASER EXPERIMENTS

In contrast to synchrotron operations an XFEL delivers packages of ultrashort monoenergetic X-rays with a spread in time from 1 fs to 100 fs. Counting individual photons is no longer possible. On the time resolution scale of a detector all X-ray photons of one shot arrive at the "same time". The charge signal amplitude in each pixel has to be measured precisely to obtain the number of X-ray hits per pixel per shot. The basic set-up is shown in Fig. 8. An X-ray pulse from the undulators of the FEL is interacting e.g., with nanocrystals or viruses injected into the interaction region with the help of a water or aerosol jet. Up to $10^{13}$ X-rays of 1.8 keV in the experiment described here[12,13] are hitting the sample within a few femtoseconds and destroying it. Almost all electrons of the sample atoms are stripped off and the sample undergoes "Coulomb" explosion. If the X-ray pulse is short enough (Δ t

< 50 fs) the diffracted X-rays carry the initial diffraction information of the sample before Coulomb explosion destroys it. This process is called: diffraction before destruction. During the experiments at the Linac Coherent Light Source (LCLS) in Menlo Park the X-ray laser was operated with repetition rates up to 120 Hz. The readout of the detector had to be finished within 8 ms[14]. Fig. 8 shows the basic concept of the Atomic, Molecular & Optical Science beamline (AMO) end station at the Linac Coherent Light Source (LCLS) in Menlo Park used for the analysis of nanocrystals of the photosystem I[12]. The detector system consists of two sets of pnCCDs, the front and the rear pnCCD. In the front pnCCD detector the powder-diffraction type image was recorded and simultaneously the small angle scattering image in the rear detector. Diffraction peaks from the data were identified, indexed and combined into a set of 3D structure factors[12]. Currently, six X-ray laser facilities are operating worldwide with concepts similar to the above described one at LCLS. To obtain information about structure and dynamics of biological samples[13] an additional advantage by using X-ray lasers is that samples do not need to be cooled like in cryo-TEMs. Biological objects may change their properties if refrigerated to cryogenic temperatures. Fig. 9 shows the recorded diffraction pattern of the mimivirus and the 2D reconstructed shape of the virus in real space with a spatial resolution of less than 20 nm.

## LABORATORY USE OF 2D SPECTROSCOPIC IMAGERS

In contrast to the large infrastructures mentioned above (satellites, synchrotrons and X-ray FELs) the use of 2D energy, position and time resolving imagers in laboratories is widely spread. Conventional X-ray sources, microfocus sources with multilayer optics or polycapillary lenses and liquid metal jet sources are delivering less X-ray fluence but more experimental liberty. If X-ray energies above 2 keV are used many measurements can be carried out in ambient conditions, i.e., without requiring vacuum. We will present two examples of laboratory experiments with energy resolving X-ray cameras.

## FULL FIELD XRF

A schematic Full Field XRF (FF XRF) set-up is shown in Fig. 10. It consists of a polychromatic X-ray source shining of the device under test, a polycapillary optics and a 2D energy resolving detector. Fluorescent X-rays from the sample excited by the X-ray source are isotropically emitted. As the polycapillary acts as a "wave guide" under total reflection conditions the original direction of the emission of the X-rays from the sample is conserved. This way a two-dimensional element resolving map can be generated as shown in Fig. 11. In this simple example a back-illuminated SIM card was analyzed[15]. The recorded spectrum and the color-coded element

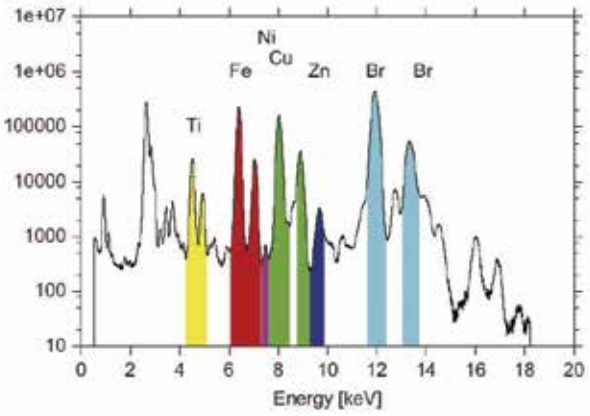


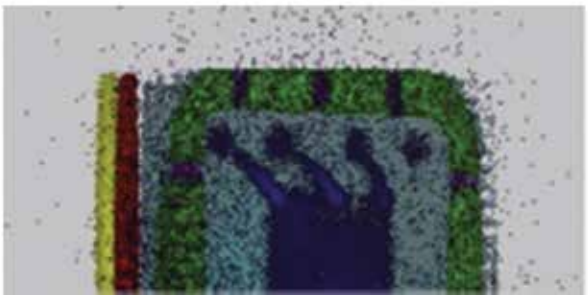

**FIGURE 11** *Elemental map of a SIM card. The spatial distribution of the various elements can be detected and displayed in real-time. The full elemental image appears from the beginning as the entire sample is illuminated by the polychromatic source and imaged through the polycapillary optics[15]. With the increasing counting statistics the image improves continuously. No scanning or movement of the camera, the X-ray source or the sample is required.*

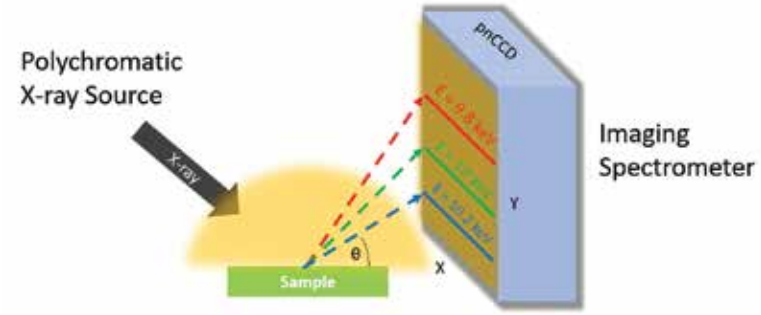


**FIGURE 12** *The simultaneous measurement and parallel analysis separate fluorescence and diffraction signals. It allows for the crystallographic characterization of an unknown sample including its elemental composition. As the fluorescence light is emitted isotropically it irradiates the pnCCD over the full area almost homogeneously. The diffracted X-rays obey Bragg´s law and are emitted under specific angles depending on their energy and lattice spacing of the sample.*

map is illustrated in Fig. 11. This technique is a powerful tool for quality control and assurance in industrial applications.

The FF-µXRF technique satisfies equally the requirements of artists and archeologists for imaging and analysis of objects of cultural heritage[16]. It allows analysts to quickly identify critical areas and hidden structures, with the advantage that the imaging technology is extremely similar to other cameras commonly used for optical, UV-VIS and NIR imaging.

The final result of the FF XRF is always an image that contains spatial and spectroscopic information. The X-ray camera is equally used for Proton Induced X-ray Emission (PIXE)[17], Double Dispersive X-ray Fluorescence ($D^2XRF$)[18] and the analysis of archeological objects[16]. For the operation in air thin external radiation entrance windows can be integrated to prevent contamination of the camera. Typically, thin Be or polymer windows are used or the more recent $Si_3N_4$ based blocking filters with high transmission of X-rays down to 500 eV.

## SIMULTANEOUS FLUORESCENCE AND DIFFRACTION

The simultaneous detection of fluorescence and diffraction X-rays provides a wealth of information about the nature of the sample under test. For the analysis of materials in terms of elemental composition and crystallographic structure a new method was presented in 2016[19]. The basic set-up is shown in Fig. 12.

Addressing a micro-focused X-ray beam to a sample and recording the X-ray fluorescence spectrum using an energy dispersive detector has long been used as a microanalytical technique, known commonly as µXRF.

Similarly, if the same focused X-ray beam is addressed to a sample in the forward scattering geometry (Bragg-Brentano) and a θ – 2θ scan is performed, a diffraction pattern can be recorded, and the technique is known as µXRD. In both cases, an image can be created by recording data at an array of equally spaced points on the sample, which is typically accomplished by moving the sample with a motorized stage.

However, if both diffraction and fluorescence data are required, then these measurements are usually made in separate instruments. The technique of µXRF imaging can be quite fast, but µXRD imaging, because it requires a θ – 2θ scan at each point, can take days. Energy dispersive

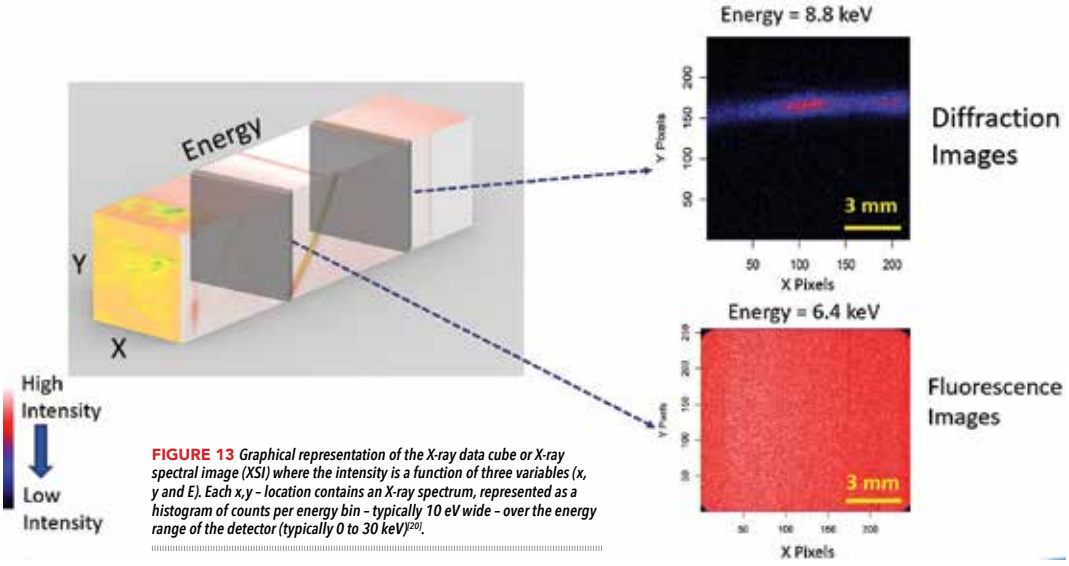


**FIGURE 13** *Graphical representation of the X-ray data cube or X-ray spectral image (XSI) where the intensity is a function of three variables (x, y and E). Each x,y – location contains an X-ray spectrum, represented as a histogram of counts per energy bin – typically 10 eV wide – over the energy range of the detector (typically 0 to 30 keV)[20].*

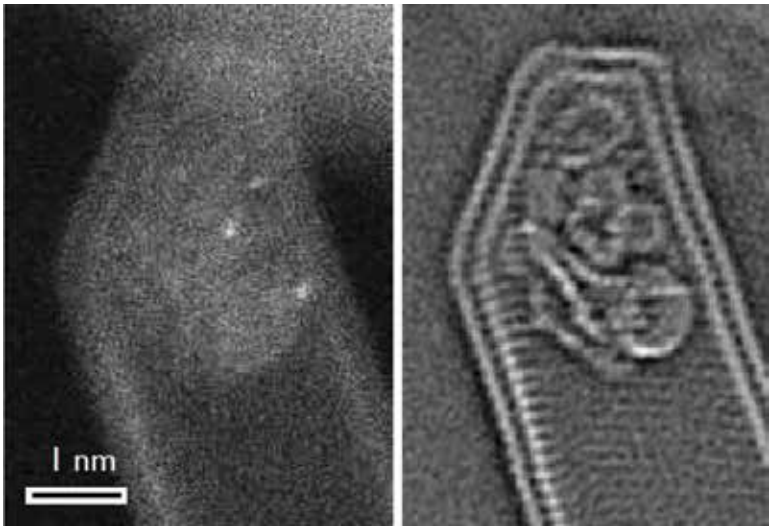


**FIGURE 14** *Electrons recorded in a TEM directly with a pnCCD camera. The annular dark field (ADF) image with high Z-contrast (left) and phase image (right) of a double-wall carbon nano tube sample (CNT) containing iodine atoms, recorded simultaneously. The reconstructed phase image after correcting the residual aberrations of the sample used ptychography methods described in*[22].

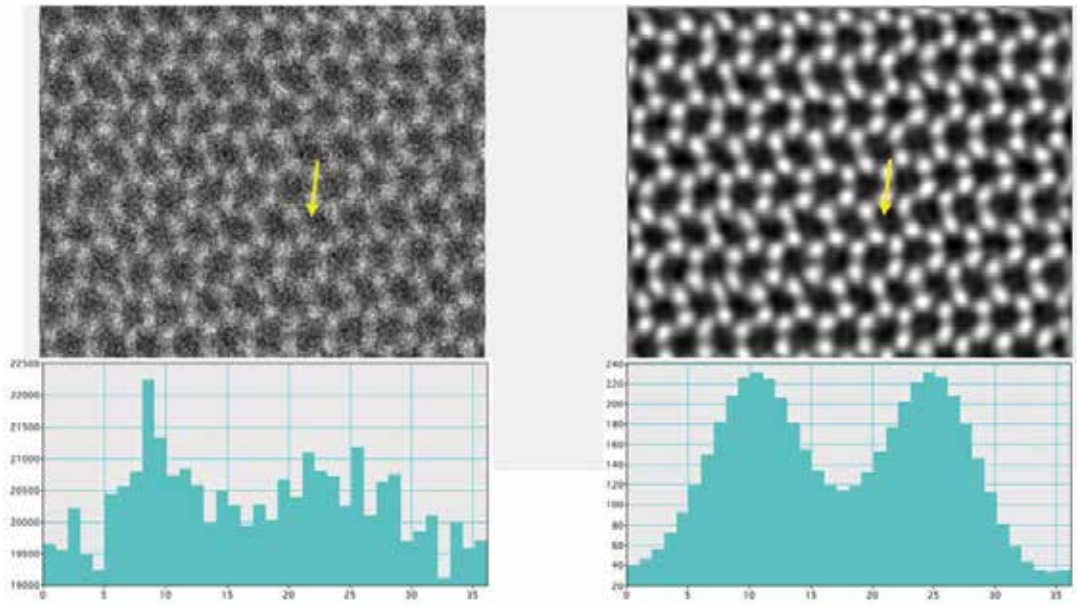

**FIGURE 15** *TEM images of a graphene sample recorded with a pnCCD camera. Comparison of the reconstructed phase (right) and the conventional annular dark field (ADF) image (left) of a graphene sample using ptychography methods. The images – simultaneously recorded – contain 256x256 probe positions recorded with a dwell time of 500 µs, corresponding to a total acquisition time of 35 s. The line profiles clearly show the tremendous improvement in spatial resolution.*

X-ray diffraction (EDXRD) enables the analysis of a wide range of d-spacings without the need for a θ – 2θ scan, but this technique is difficult to use if the sample is compositionally complex, since the fluorescence and diffraction peaks frequently overlap. This problem can be mitigated through the use of an imaging spectrometer, such as the pnCCD[15].

The Color X-ray Camera (CXC) with its integrated pnCCD is capable to measure the position and energy of each X-ray photon hitting the detector. The three-dimensional X-ray spectrum image (XSI) with x, y and energy values in Figure 13 has been recorded from such data[20].

This method can be further enhanced by addressing a micro-focused X-ray beam to an array of points on a given sample and recording an XSI at each point, producing a five-dimensional dataset with ($X_{sample}$, $Y_{sample}$, $X_{camera}$, $Y_{camera}$ and energy) enabling for a rapid off-line analysis.

## DIRECT DETECTION OF ELECTRONS IN (S)TEM

Advances in fast pixelated detector technology have enabled coherent diffraction patterns in a scanning transmission electron microscope (STEM) to be recorded at every probe position to form a four dimensional (4D-) STEM dataset (($X_{sample}$, $Y_{sample}$, $X_{camera}$, $Y_{camera}$) The rich information contained in the 4D-STEM dataset has previously been poorly utilized by the STEM bright-field detector with a small collection angle, hindering the efficiency for imaging light elements. Furthermore, collecting the electron intensity using integrating detectors such as annular bright field and the annular dark field (ADF) detectors is not able to make full use of the diffraction information.

Electron ptychography is a method for retrieving phase information using diffraction patterns acquired from a sequential array of overlapping illuminated areas, and has been first demonstrated on a 4DSTEM dataset more than 20 years ago for improving image resolution[21]. At that time, the image field of view was restricted by the limitations of the camera speed and computational processing power. Using a modern aberration-corrected STEM and a fast pixelated detector, quantitative phase images can be formed simultaneously with other STEM imaging modes such as ADF at atomic resolution[22]. This phase imaging mode has a monotonic phase contrast transfer function and provides an inherent filter of image noise without reducing the strength of the phase contrast. It was shown that the large redundancy in phase information in the 4D-STEM data not only offers efficient phase imaging, but also allows lens aberrations to be detected and corrected through post-acquisition processing (Fig.14) by applying a ptychography method called Wigner-distribution deconvolution (WDD).

The aberration measurement and correction method works on both amorphous and crystalline specimens. Moreover, three-dimensional structure information is also available post-acquisition by reconstructing the phase image at a specific depth in the specimen along the e-beam direction, which can be performed even though the microscope may not have been focused at that depth.

The full and direct detection of energetic electrons in an energy range of 10 keV and 300 keV is requiring different sensor properties as compared to X-rays. The absorption depth of a 10 keV electron is less than 1 µm while a 300 keV electron has a projected range of over 400 µm. In addition, the detector and its radiation entrance window have to be highly radiation tolerant. A high readout speed, high dynamic range, low noise and good spatial resolution are equally important parameters. These features have been addressed for the implementation of the pnCCD as a 4D (S)TEM camera. Especially for the sub – Å resolution analysis performed with ptychographic methods the pnCCD is well established in various laboratories.

The electrons of a focused beam interact with one point on the sample and generate a diffraction image on a 2-dim electron detector depending on the settings of the TEM of the order of 1 $cm^2$. In a subsequent step the electron beam is displaced such that the diffraction pattern partially overlaps with the previous one. This way the relative phase can be retrieved and used for the reconstruction of the sample structure as can be seen in Fig. 15. The image is the annular dark field (ADF) image with the corresponding line profile below. The tremendous improvement in image quality can be seen in the right part of Fig. 15 with the corresponding line profile below[22]. As low dose measurements above 120 keV become increasingly relevant the performance figures for a direct electron detector move towards even higher readout speed and precise determination of the point of entry of the TEM electrons at the detector's radiation entrance window.

## SUMMARY AND CONCLUSIONS

The introduction of the principle of sideward depletion by Gatti and Rehak in 1983, what is now known as the silicon drift detector (SDD) has had an important influence on the detection of ionizing radiation in a large number of scientific instruments utilized in basic and applied science experiments as well as industrial applications. The pixelated relatives of the SDDs, the pnCCD have opened a new series of prominent applications in basic and applied science. Their key properties include high efficiency for X-rays from 1 eV to 30 keV and electrons up to 300 keV, Fano-limited energy resolution, fast readout, high spatial precision and excellent long-term stability. Future developments include back illuminated active pixel sensors fabricated on fully depleted semiconductors with very thin intrinsic radiation entrance windows.

**Article, videos and references available online at: analyticalscience.wiley.com/publication/microscopy-and-analysis**